Title
nN DATA COMPILATION AND AMALGAMATION

Authors
Hodgkinson, D.P.
Kelly, R.L.
Cutkosky, R.E.
et al.

Publication Date
1974-06-01

Submitted to the 17th International Conference
on High Energy Physics, London, England,
July 1-10, 1974

LBL-3048
c.2

πN DATA COMPILATION AND AMALGAMATION

D. P. Hodgkinson, R. L. Kelly, R. E. Cutkosky,
and J. C. Sandusky

June 1974

Prepared for the U. S. Atomic Energy Commission
under Contract W-7405-ENG-48

LBL-3048
c.2

DISCLAIMER

LBL-3048

πN Data Compilation and Amalgamation

D.P. Hodgkinson and R.L. Kelly
Lawrence Berkeley Laboratory, Berkeley, California

R.E. Cutkosky and J.C. Sandusky
Carnegie-Mellon University, Pittsburgh, Pennsylvania

Submitted to the 17th International Conference on High Energy Physics
1 to 10 July 1974, Imperial College, London

Abstract

We are compiling and amalgamating πN elastic and charge exchange scattering data in the resonance region. Preliminary results in the 1-2 GeV/c region are presented in this paper. The compilation procedure involves checking and correcting the Lovelace-Almehed 1971 data collection, as well as collecting all more recent data. Each set of compiled data of the six extant types (elastic and CEX cross sections and polarizations) is amalgamated in momentum bins about 50 MeV/c wide. The amalgamation is done by fitting a momentum and angle dependent surface to the data over a momentum range of about 3 bin widths, using the fitting surface in the central bin to shift the data into fixed angular bins at a predetermined central momentum, and then statistically combining the data in each bin. The fitting procedure takes into account normalization errors, calibration errors and resolution of beam momenta, electromagnetic corrections, and inconsistent data. The central bins and central momenta for each type of data are identical, thus reducing the number of points at which amplitudes need be calculated in a partial wave analysis program using the amalgamated data. The errors of interpolation are greatest for CEX data, since they are the least abundant, so the central momenta have been chosen to reduce the amount of interpolation of CEX data. The amalgamated data are correlated, but we have found that the correlations can be accurately parameterized in such a way that, rather than necessitating double sums over each type of data in a fitting program, they can be represented in terms of three single sums.

I. Introduction

Pion-nucleon elastic and charge-exchange scattering are the most extensively studied processes in high energy physics. Well over 100 cross section and polarization experiments have been performed in the resonance region alone. The use of this data in the planning of further experiments, partial wave analysis programs, theoretical calculations, etc. is difficult for a number of reasons. Besides the labor involved in simply collecting the data, there are many problems associated with differences in the running conditions of the various experiments leading to systematic discrepancies in each type of data. Some of these discrepancies come from known, correctable effects (small mismatches in beam momenta, normalization errors, etc.) while some are due to experimental biases of unknown origin and persist after all known effects are taken into account. In addition, simultaneous use of several types of data in an energy independent fitting program requires binning in momentum, introducing an unknown amount of bias, and further binning in angle may be necessary to reduce computing expense.

The project described here is an attempt to solve these problems and to present "amalgamated" data in an accurate and economically useable form. The general procedure used is to fit the world data of a given type over a momentum range of about 150 MeV/c with a momentum and angle dependent surface, and then to shift the data in a central momentum bin about 50 MeV/c wide along the surface to the nearest of a set of prechosen angles (referred to here as angular "bins") at a prechosen central momentum. The angular bins are chosen to be evenly spaced at intervals of 3°, 61 bins in all. We use fixed angle spacing in order to make the bins more closely packed in cos θ in the forward and backward peaks than in the wide angle region. The central momenta are chosen to match the momenta of existing charge-exchange (CEX) data as nearly as possible because these data are particularly susceptable to interpolation error. During the fitting inconsistencies among the data are taken into account by enlarging the errors of discrepant data. After shifting, the data in each bin is statistically combined. The remainder of this paper describes the various steps of the amalgamation process in more detail, and presents preliminary results in the 1-2 GeV/c region.

II. Compilation Procedure

The most extensive existing collection of pion nucleon elastic and CEX scattering data is the Lovelace-Almehed data tape.[1] This tape is complete through September 1972, and we have used it as a basis for our compilation. Data from the tape is first transferred to cards and corrected for "systematic" mistakes, e.g., missing data, preliminary data quoted as final data or along with final data, data copied from the wrong table in a publication, etc. Data from other sources, primarily post-1972 publications and private communications of unpublished data,are also stored on cards. After a convenient amount of data has been obtained (typically 2K to 3K data points) it is written onto a single file of a binary tape in a standard format, and printed out for proof-reading. Corrections found by the proof-reader are made using an editing program, and the contents of the file are then transferred to chipstore (an LBL on-line photo-digital storage system). Any revisions found to be necessary after this stage are also made by the editing program. The chipstore files are collected together into a single binary tape file for use in the amalgamation program described below.

III. Fitting Procedure

The momentum and angle dependent interpolating surface for each type of data in each momentum bin is determined by minimizing

$$\chi^2 = \chi^2 + \Phi \qquad (1)$$

where

$$\chi^2 = \sum_{\epsilon i} \frac{w_{\epsilon i}}{s_{\epsilon i}^2}\left(\lambda_\epsilon f_{\epsilon i} - s_{\epsilon i} d_{\epsilon i}\right)^2 + \sum_{\epsilon\eta} w^1_{\epsilon\eta}(\lambda_\epsilon - 1)(\lambda_\eta - 1) + \sum_{\epsilon\eta} w^2_{\epsilon\eta}(q_\epsilon - p_\epsilon)(q_\eta - p_\eta)$$

and Φ is a convergence test function (see below). We use the following notation:

$\epsilon, \eta, \ldots$ denote blocks of data from a single momentum of a single experiment.

$d_{\epsilon i}$ is the value of the i^{th} datum of block ϵ. In the case of cross section data a single photon exchange scattering and interference term, $c_{\epsilon i}$, is subtracted from the data before fitting and added back in at the shifted position.

$s_{\epsilon i}$ is unity for cross section data, and is the fitted cross section divided by sin θ at the position of datum ϵi for polarization data. Multiplication by this factor gives both quantities the same analyticity properties.

p_ϵ is the published beam momentum of block ϵ.

$w_{\epsilon i}$ is the inverse square error of datum ϵi.

$w^1_{\epsilon\eta}$ is the inverse covariance matrix of the experimental normalizations. Relative normalizations, where known, are taken into account by appropriate off-diagonal elements.

$w^2_{\epsilon\eta}$ is the inverse covariance matrix of the beam momenta. Off-diagonal elements are constructed on the assumption that published beam momentum errors are primarily overall calibration errors common to all momenta from a given experiment, but are also subject to an irreproducable "jitter" at each individual momentum. Except in the few cases where detailed information is available, we have been forced to guess at the jitter and have used ±2 MeV/c.

$f_{\epsilon i}$ is the fitted value corresponding to datum ϵi (see below).

λ_ϵ is the inverse fitted normalization of block ϵ. The use of an inverse normalization factor in this way is equivalent to the use of a direct scale factor to first order in deviations from unity, and is done here to simplify the χ^2 function.

q_ϵ is the fitted beam momentum of block ϵ.

The fitted values are parameterized as polynomials in the beam momentum and an angular variable z:

$$f_{\epsilon i} = \sum_m a_m T_{m\epsilon i}$$

Here the a_m are fitted coefficients and $T_{m\epsilon i}$ is a polynomial corrected for the momentum resolution of the ϵ^{th} beam,

$$T_{m\epsilon i} \equiv T_m(z_{\epsilon i}, q_\epsilon) + \frac{1}{2} b_\epsilon^2 \frac{\partial^2 T_m(z_{\epsilon i}, q_\epsilon)}{\partial q_\epsilon^2}$$

where b_ϵ is the momentum bite half-width for data block ϵ interpreted as the RMS deviation of the beam momentum spectrum from its central value. The angular variable z is chosen to map the cos θ plane into a unifocal ellipse with the right- and left-hand singularities on the preiphery and the physical region between the focii[2]. This mapping stretches the physical region in the forward and backward peaks while compressing it in the wide angle region, thus tending to produce flatter structure in z than in cos θ and to reduce the number of terms required for a good fit. The highest order polynomials T_m that contribute appreciably to the fit are typically about 8th order in z, and are at most quadratic in q. More is said below about how the polynomials are actually chosen.

The convergence test function (CTF) is used to effect a smooth cutoff in the number of expansion coefficients a_m used in the fit[3]. It is constructed by first separating the momentum and angle dependence of the fitting function,

$$f(z,q) \equiv \sum_m a_m T_m(z,q) = \sum_n y^n f_n(z)$$

where $y = (q - \bar{q})/q_0$, $\bar{q}$ is a weighted average of the beam momenta, and q_0 acts as a cutoff parameter for the momentum dependence. The CTF is then,

$$\Phi = C \sum_n \oint_{ellipse} \left| \frac{dz}{\sqrt{1-z^2}} \right| |f_n(z)|^2$$

The higher powers of z are magnified with respect to the lower powers on the boundary of the ellipse, so addition of this term to χ^2 cuts off these higher powers smoothly. The region in which the cutoff becomes effective is controlled by adjusting C. By carrying out the integrals Φ can be expressed in terms of a "truncation matrix", $\mathcal{J}_{mn}$.

$$\Phi = \sum_{mn} \mathcal{J}_{mn} a_m a_n$$

The particular weight function used in the integral is chosen because Tchebichef polynomials are orthogonal with respect to this weight and this facilitates computation of Φ.

The number of data points in a 150 MeV/c wide momentum bin can approach 1000 for the more copious data types, and the total number of variable parameters a_m, λ_ϵ, q_ϵ is sometimes as large as 100. Thus, to reduce expense and to handle error propagation more accurately, we have written a minimizer tailored to our χ^2 function rather than using an existing general purpose minimizer. The minimization procedure is iterative and alternates between two basic types of steps. The first type is a generalization of orthogonalized least squares in which the fitted normalizations and momenta (referred to collectively below as shift parameters), are held fixed while the polynomials T_m and their coefficients are adjusted to minimize χ^2. The polynomials are chosen to satisfy the orthogonality relation,

$$\sum_{\epsilon i} \lambda_\epsilon^2 W_{\epsilon i} T_{m\epsilon i} T_{n\epsilon i} + \mathcal{J}_{mn} = \delta_{mn}$$

and the coefficients are then

$$a_m = \sum_{\epsilon i} \lambda_\epsilon W_{\epsilon i} d_{\epsilon i} T_{m\epsilon i}$$

In the second type of step the polynomials are held fixed and all the parameters are simultaneously varied to find an approximate minimum by Newton's method. This requires inversion of the second derivative matrix of X^2, and this is simplified by the orthogonality relation imposed in the previous step. The calculation of the inverse is also useful later on for error propagation. (In addition to these basic steps safeguards are provided against the well known instabilities of Newton's method, and some other types of steps are used early in the iteration to optimize the program.)

A useful byproduct of this procedure is the ability to calculate the effective number of coefficients used in fitting each data point. If datum ϵi is omitted and X^2 is reminimized, holding the shift parameters fixed but varying all the coefficients, the resulting decrease in X^2 is,

$$\Delta_{\epsilon i} = \frac{\chi^2_{\epsilon i}}{1 - \omega_{\epsilon i}}$$

where $\chi^2_{\epsilon i}$ is the contribution of datum ϵi to X^2 in the original fit and

$$\omega_{\epsilon i} = \lambda_\epsilon^2 W_{\epsilon i} \sum_m T^2_{m\epsilon i}$$

The quantity $\omega_{\epsilon i}$ satisfies the "sum rule"

$$\sum_{\epsilon i} \omega_{\epsilon i} = N_c - \mathrm{Tr}\, \mathcal{J}$$

where N_c is the total number of coefficients, and is naturally identified with the effective number of coefficients used in fitting datum ϵi. The quantity Tr $\mathcal{J}$ can be identified with the effective number of coefficients held fixed by smoothness constraints.

IV. Error Adjustment

The chi-squared confidence levels of fits obtained as described in the previous section are often very small. This is due to unknown experimental biases and errors in some of the data, and these effects will propagate into the amalgamated data unless they are explicitly removed. The nature of the problem is illustrated by plotting histograms of the data point and data block confidence level distributions calculated on the assumption of Gaussian errors. Examples are shown in Fig. 1. Instead of being flat, the distributions are peaked at low confidence levels. These peaks are nearly always present though their heights and widths vary from bin to bin. The data block confidence level distribution is usually even more sharply peaked than that of the data points, indicating a fairly even scattering of bad data among the different blocks.

We deal with this problem by doing the X^2 minimization in two passes. After the first pass error bars of data in the low confidence level peak are stretched as described below, and the data is then refit. After the second fit the stretching is done again, but at this stage the low confidence level peak has essentially disappeared so the effect is minor. The stretching algorithm is defined in terms of

$$\tilde{\chi}^2_{\epsilon i} = N_d \chi^2_{\epsilon i} / N_f$$

where N_d is the number of data points (including normalizations and momenta) and

$$N_f = N_d - N_s - \sum_{\epsilon i} \omega_{\epsilon i}$$

is the effective number of degrees of freedom (N_s is the number of shift parameters contributing to χ^2). The quantities $\tilde{\chi}^2_{\epsilon i}$, and similarly defined quantities for the normalizations and momenta, are expected to be distributed approximately in a chi-squared distribution for one degree of freedom if the errors are truly Gaussian; these are the quantities used to generate the histograms in Fig. 1. The error $e_{\epsilon i}$ of datum ϵi is stretched according to the algorithm,

$e_{\epsilon i}$ unchanged if $\tilde{\chi}^2_{\epsilon i} < \delta_0^2$

$$e_{\epsilon i} \rightarrow e_{\epsilon i}\left[1 + (\delta_1 - 1)\left(\frac{\sqrt{\tilde{\chi}^2_{\epsilon i}} - \delta_0}{\delta_1 - \delta_0}\right)^2\right] \quad \text{if} \quad \tilde{\chi}^2_{\epsilon i} > \delta_0^2$$

and a similar procedure is applied to the normalization and momentum covariance matrices. Thus stretching begins when $\tilde{\chi}^2_{\epsilon i}$ exceeds δ_0^2, and becomes extreme when $\tilde{\chi}^2_{\epsilon i}$ exceeds δ_1^2; δ_0 and δ_1 are chosen to lie near the edge and the middle of the low confidence level peak, respectively. Typical values are $\delta_0 = 2$ and $\delta_1 = 3$-4. About 10% of the errors are usually adjusted by this algorithm.

Provision is also made for simultaneous stretching of all the error bars in data blocks that remain poorly fit after the above procedure is carried out, but this is seldom necessary and the overall stretching factor is never larger than about 1.2.

V. Interpolation and Averaging

After the fitted surface has been determined, data in a central momentum bin ~1/3 as wide as the whole range covered by the fit is renormalized and shifted into fixed angular bins at a central momentum, q_c. A shifted datum is,

$$D_{b\epsilon i} = \frac{f_b}{s_b} + r_{b\epsilon i}\left(\frac{d_{\epsilon i}}{\lambda_\epsilon} - \frac{f_{\epsilon i}}{s_{\epsilon i}}\right) + c_b$$

where b denotes the bin into which datum ϵi is shifted, s_b is defined similarly to $s_{\epsilon i}$, c_b vanishes for polarization data and is defined similarly to $c_{\epsilon i}$ for cross section data, $r_{b\epsilon i}$ is unity for cross section data and is $\sin\theta_b / \sin\theta_{\epsilon i}$ for polarization data, and

$$f_b = \sum_m a_m T_{mb}$$

where

$$T_{mb} = T_m(z_b, q_c)$$

Thus, the renormalized cross section data is moved parallel to the fitted surface while the deviation of the renormalized polarization data from the fitted polarization is modulated by sin θ. Note that the beam momentum resolutions are also unfolded at this point.

The covariance matrix of the shifted data is obtained by calculating the effect on the results of fluctuations in the input data. We consider a generalized X^2 function, X_g^2, of which (1) is supposed to be a special case:

$$X_g^2 = \sum_{\epsilon i} \frac{\tilde{w}_{\epsilon i}}{s_{\epsilon i}^2} \left(\lambda_\epsilon f_{\epsilon i} - s_{\epsilon i} D_{\epsilon i}\right)^2 + \sum_{\epsilon\eta} \tilde{w}^1_{\epsilon\eta} (\lambda_\epsilon - \Lambda_\epsilon)(\lambda_\eta - \Lambda_\eta)$$

$$+ \sum_{\epsilon\eta} \tilde{w}^2_{\epsilon\eta} (p_\epsilon - P_\epsilon)(p_\eta - P_\eta) + \sum_{mn} \mathcal{J}_{mn} (a_m - A_m)(a_n - A_n)$$

Here $D_{\epsilon i}$, Λ_ϵ, P_ϵ, and A_m are considered to be Gaussian randomvariables which have the particular values $d_{\epsilon i}$, 1, $p_{\epsilon i}$, and 0 in (1), have some unknown mean values, and have inverse covariance matrices $\tilde{w}_{\epsilon i}$ (diagonal), $\tilde{w}^1_{\epsilon\eta}$, $\tilde{w}^2_{\epsilon\eta}$, and $\mathcal{J}_{mn}$, respectively. The matrices $\tilde{w}$, $\tilde{w}^1$, and $\tilde{w}^2$ are the original matrices w, w^1, and w^2 as modified by error bar stretching. The treatment of the CTF in this way is a formal device for taking into account its effect in damping fluctuations in the higher order terms. To now propagate fluctuations in the random input variables into the shifted data we must make some guess for the mean values, and we have identified these with the fitted values. As a test of the sensitivity of this assumption we have done calculations with some of the mean values identified with the input values and found negligible differences.

The error propagation calculation does not take into account the effect of fluctuations in the input cross section data on the shifted polarization data through the factor $s_{\epsilon i}$. We neglect this effect because the cross section data are generally considerably more precise than the polarization data. Tests have been made to check that the effect is in fact negligible. We also neglect fluctuations in the adjusted inverse covariance matrices $\hat{w}$, $\hat{w}^1$, and $\hat{w}^2$.

The resulting covariance matrix of the shifted data is,

$$V_{b\epsilon i, d\eta j} = \delta_{b\epsilon i, d\eta j} \frac{r_{b\epsilon i}}{\lambda_\epsilon^2 \tilde{w}_{\epsilon i}} - \frac{r_{b\epsilon i}\, r_{d\eta j}}{s_{\epsilon i}\, s_{\eta j}} \left\{ \frac{1}{\lambda_\epsilon \lambda_\eta} \sum_{gh} U_{\epsilon g, \eta h} f_{\epsilon i g} f_{\eta j h} \right.$$

$$+ \frac{1}{\lambda_\epsilon} \sum_{gm} U_{\epsilon g, m} f_{\epsilon i g} T_{m \eta j} + \frac{1}{\lambda_\eta} \sum_{gm} U_{\eta g, m} f_{\eta j g} T_{m \epsilon i}$$

$$\left. + \sum_{mn} U_{mn} \left(T_{m\epsilon i} T_{n\eta j} - \frac{s_{\epsilon i} s_{\eta j} T_{mb} T_{nd}}{r_{b\epsilon i} r_{d\eta j} s_b s_d} \right) \right\}$$

where U is the covariance matrix of the fitted parameters obtained from the second derivative matrix of X_g^2 with the above mentioned identification of mean values and fitted values. The indices g and h take the values 1 and 2 denoting normalization and momentum shift parameters, respectively, when used with U. Also,

$$f_{\epsilon i 1} = f_{\epsilon i}$$

$$f_{\epsilon i 2} = \lambda_\epsilon \frac{\partial f_{\epsilon i}}{\partial p_\epsilon}$$

The first term of V is primarily due to the errors of the original data while the remaining terms represent errors of renormalization, momentum shifting, and interpolation. These latter errors are generally somewhat smaller than, but comparable to, those of the original data.

Amalgamated data is now made by forming a weighted average of the data in each bin,

$$D_b = \sum_{\epsilon i}^{b} \gamma_{b\epsilon i} D_{b\epsilon i}$$

where $\gamma_{b\epsilon i}$ is chosen to minimize the variance of D_b,

$$\gamma_{b\epsilon i} = \sum_{\eta j}^{b} W^b_{\epsilon i, \eta j} \Big/ \sum_{\delta k, \eta j}^{b} W^b_{\delta k, \eta j}$$

Here w^b is the inverse of the submatrix of V pertaining to bin b. The covariance matrix of the amalgamated data is,

$$A_{bd} = \sum_{\epsilon i}^{b} \sum_{\eta j}^{d} \gamma_{b\epsilon i} \gamma_{d\eta j} V_{b\epsilon i, d\eta j}$$

The existence of correlations between the amalgamated data tends to make them somewhat more complicated and expensive to use than ordinary, uncorrelated, experimental data. The calculation of x^2 in a fitting program, for example, would require a double sum over the data if the full covariance matrix were used. To alleviate this complication we have attempted to find simple ways to parameterize the correlations. Two acceptable parameterizations have been found. Both are based on approximating the full covariance matrix by a simpler matrix $\tilde{A}_{bd}$ with the same diagonal elements. The free parameters of $\tilde{A}_{bd}$ are determined by minimizing the mean squared value of the off-diagonal elements of the residual correlation matrix,

$$r_{bd} = \frac{A_{bd} - \tilde{A}_{bd}}{(A_{bb} A_{dd})^{1/2}}$$

The two parameterizations we have used are,

$$\tilde{A}_{bd} = \epsilon_b^2 \delta_{bd} + n^2 f_b f_d / S_b S_d$$

and

$$\tilde{A}_{bd} = \delta_{bd} / W_b + K^1_b K^1_d + K^2_b K^2_d$$

In the first case the data may be treated as uncorrelated with errors $\pm \epsilon_b$ and an overall normalization error $\pm$ n (as long as $n^2 << 1$). In the second case we choose the "correlation vectors" K^1 and K^2 to satisfy,

$$\sum_b W_b K^1_b K^2_b = 0$$

so that the inverse covariance matrix is,

$$\tilde{A}^{-1}_{bd} = \delta_{bd} W_b - W_b W_d \sum_n \beta_n^2 K^n_b K^n_d$$

where

$$\beta_n^2 = \left[1 + \sum_b W_b (K_b^n)^2 \right]^{-1}$$

Thus an approximate x^2 function, $\tilde{x}^2$, with respect to some fitted function F,

$$\tilde{\chi}^2 = \sum_{bd} \tilde{A}^{-1}_{bd} (F_b - D_b)(F_d - D_d) \qquad (2)$$

reduces to three single sums.

Another way to formulate the parameterization of $\tilde{A}_{bd}$ in terms of correlation vectors is to introduce auxiliary variables ξ_n, and use the x^2 function,

$$\tilde{\chi}^2 = \sum_b W_b \left(F_b - D_b - \sum_n \xi_n K_b^n \right)^2 + \sum_n \xi_n^2$$

Minimization of this x^2 function with respect to the ξ_n, for fixed values of the fitted function, gives the values

$$\bar{\xi}_n = \beta_n^2 \sum_b W_b K_b^n (F_b - D_b)$$

for the ξ_n. The value of $\tilde{x}^2$ at this minimum is,

$$\tilde{\chi}^2 = \sum_b W_b (F_b - D_b)^2 - \sum_n \bar{\xi}_n^2 / \beta_n^2$$

which is equivalent to Eq.(2). The advantage of this formulation is that we can interpret the ξ_n as representing collective adjustments of the data which take into account the main effects of the original shift parameters. Thus in an application, the quantities

$$\bar{D}_b = D_b + \sum_n \bar{\xi}_n K_b^n$$

can be considered as readjusted data analagous to the renormalized data obtained in applications using the first method for parameterizing $\tilde{A}$.

The second method is more complicated than the first, but is also more accurate. RMS values of the off-diagonal elements of r are seldom larger than .1, with either mothod, and with the second method are usually about half as large as with the first. One can also estimate the error made by the use of $\tilde{A}$ in Eq. (2) by regarding the D_b as Gaussian random variables with covariance matrix A and means equal to the values F_b at minimum. This gives a mean and central variance for x^2 of Tr $\tilde{A}^{-1}$ A and 2 Tr $\tilde{A}^{-1}$ A $\tilde{A}^{-1}$ A, respectively. The bias, Tr $\tilde{A}^{-1}$ A - N_0 (where N_0 is the number of occupied bins), is seldom larger than .5; the central variance seldom exceeds $2N_0$ by more than 20% and the discrepancy with the second method is usually about half as much as with the first.

VI. Results

The main elastic and CEX scattering experiments in the 1-2 GeV/c region are surveyed in Table I.[4] As a simple measure of the quantity and quality of the data of each experiment we have calculated "weights" equal to the sum over data points of the inverse square fractional errors for cross section data and equal to the sum of the inverse square absolute errors for polarization data. If the errors were purely statistical, weights defined in this way would be equal to the total number of events counted in a cross section experiment, and would at least be of this order of magnitude for a polarization experiment. In practice this is usually quite far from the truth, the weight being much smaller than the actual number of events, but it does provide a useful measure of the influence of the data in a χ^2 fit. The weights shown in Table I are summed over data in the 1 GeV/c $\leq p_{lab} <$ 2 GeV/c momentum range only. For each elastic cross section we list all experiments contributing $\gtrsim$ 3% of the total weight of measurements of that cross section in this momentum range; for the other types of measurement we list all experiments contributing $\gtrsim$ 1% of the appropriate total weight. The compilation used for this survey contains all data from experiments overlapping the 1-2 GeV/c momentum range, and nearly all of these data are included in the preliminary amalgamation results described below. In a few cases, some of the data were omitted, usually because of severe disagreement with a number of nearly measurements. Because of the error stretching feature of the amalgamation process, the final results are not much affected when severely discrepant data of this kind is dropped; changes in individual data points were observed to be $\lesssim .5\ \sigma$.

In addition to the compiled data we used 0° elastic cross section "data" calculated by combining forward imaginary parts from the total cross section measurements of Carter, et. al.[5] and forward real parts from the dispersion relation calculations of Carter and Carter[6] (interpolated to the momenta of the total cross section data). This data was used only to make the fitted surface better defined, and was not included in the shifting and averaging.

An example of the effect of amalgamation is shown in Fig. 2. The overall range of the fit for this example was 1370-1525 MeV/c; the input data shown is from a central bin between 1420 and 1465 MeV/c; the central momentum at which this data is amalgamated is 1437 MeV/c. The input cross section data consists of two data blocks from Hughes 72, and one each from Laasanen 73, Vavra 72, Kalmus 71 and two smaller experiments[7,8] not listed in Table I. The larger of these data blocks contribute comparable weights, and the amalgamated data is therefore considerably more precise than any single input data block. The input polarization data consists of single data blocks from Martin 74, Albrow 70, Chamberlain 66, and one smaller experiment[9] not in Table I. In this case, the input data is dominated by the data block from Martin 74 at 1439 MeV/c (diamond symbols in Fig. 2) and the amalgamated data is largely a reproduction of this data block in new angular bins. The remaining, less precise, input data is particularly useful in bins where Martin 74 does not contribute, e.g., the four forwardmost occupied bins and two bins where the polarization is changing rapidly near $\cos\theta = .5$.

We have amalgamated data at 22 momenta in the 1-2 GeV/c region. Specimen results at 1030, 1247, 1437, and 1790 MeV/c are shown in Figs. 3-8. These are four of the five momenta at which CEX polarization data is reported by Shannon 74; the results shown in Fig. 8 are energy independent amalgamations (essentially angular rebinnings) of this data. The errors shown in Figs. 2-8 are obtained using the normalization error type of parameterization of $\hat{A}$ discussed in the previous section.

In Figs. 9-16 we show contour maps drawn from the fitted surfaces in each of our 22 central momentum bins. These are shown for elastic cross sections, polarizations, and transverse cross sections

$$I_{\pm} = \frac{1}{2}(1 \pm P)\frac{d\sigma}{d\Omega}$$

(There is not enough data to make CEX maps.) Discontinuities in the contour lines appear at the bin edges and give some indication of the experimental errors. The π^+p maps are considerably smoother than the π^-p maps; this is largely due to the precise measurements of Laasanen 73, Hughes 72, and Martin 74.

The transverse cross sections are squares of single transversity amplitudes, and vanish where zeros of these amplitudes cross the physical region. The two most prominent features suggestive of such zero transits occur in the π^+p maps near p_{lab} =1390 MeV/c and cosθ = 0.29 for I_+ and near p_{lab} = 1630 MeV/c and cosθ = 0.56 for I_-

Acknowledgements

We wish to thank the many experimentalists who have cooperated with this project by supplying us with their data and answering detailed questions about their experimental parameters. Throughout this work we have benefited from numerous informative discussions with Professor Owen Chamberlain, Professor Herbert Steiner, and Dr. Steven Shannon.

References

1. C. Lovelace, et. al., πN Two-body Scattering Data. I. A User's Guide to the Lovelace-Almehed Data Tape, LBL-63 (April 1973).

2. R. E. Cutkosky and B. B. Deo, Phys. Rev. 174, 1859 (1968).

3. R. E. Cutkosky, Annals of Physics 54, 350 (1969).

4. The shortened experiment names in Table I consist of the first author and year of publication of the following references:

   J.M. Abillon, et. al., Phys. Letters 32B, 712 (1970).
   M.G. Albrow, et. al., Nucl. Phys. B25, 9 (1970).
   M.G. Albrow, et. al., Nucl. Phys. B37, 594 (1972).
   P.S. Aplin, et. al., Nucl. Phys. B32, 253 (1971).
   P. Borgeaud, et. al., Phys. Letters 10, 134 (1964).
   A.D. Brody, et. al., Phys. Rev. D3, 2619 (1971).
   T.A. Broome, priv. comm., 1973.
   F. Bulos, et. al., Phys. Rev. 187, 1827 (1969).
   G. Burleson, et. al., Phys. Rev. Letters 26, 338 (1971).
   A.S. Carroll, et. al., Phys. Rev. 177, 2047 (1969).
   O. Chamberlain, et. al., Phys. Rev. Letters 17, 975 (1966).
   C.B. Chiu, et. al., Phys. Rev. 156, 1415 (1967).
   C.R. Cox, et. al., Phys. Rev. 184, 1453 (1969).
   D.G. Crabb, et. al., Phys. Rev. Letters 27, 216 (1971).
   P.J. Duke, et. al., Phys. Rev. 149, 1077 (1966).
   P.J. Duke, et. al., Phys. Rev. 166, 1448 (1968).
   M. Fellinger, et. al., Phys. Rev. D2, 1777 (1970).
   R.E. Hill, et. al., Phys. Rev. D1, 729 (1970).
   R.E. Hill, et. al., Phys. Rev. Letters 27, 1241 (1971).
   C.M. Hughes, Univ. of Bristol Thesis, 1972.
   G.E. Kalmus, et. al., Phys. Rev. D4, 676 (1971).
   V. Kistiakowsky, et. al., Phys. Rev. D6, 1882 (1972).
   A.T. Laasanen, Univ. of Maryland Thesis, 1973.
   J.F. Martin, et. al., RHEL Report No. RL-74-016, 1974.
   J.E. Nelson, et. al., Phys. Letters 47B, 281 (1973).
   R.J. Ott, et. al., Phys. Letters 42B, 133 (1972).
   W.S. Risk, Phys. Rev. 167, 1249 (1968).
   R.E. Rothschild, et. al., Phys. Rev. D5, 499 (1972).
   S.R. Shannon, et. al., LBL-2641, 1974.
   J. Vavra, McGill Univ. Thesis, 1972.

5. A.A. Carter, et al., Phys. Rev. 168, 1457 (1968).

6. A.A. Carter and J.R. Carter, RHEL Report No. RL-73-024, 1973.

7. B. Deler, Orsay Thesis (CEA-R-3579), 1969.

8. J.A. Helland, et. al., Phys. Rev. 134, B1062 (1964).

9. R.D. Eandi, et. al., Phys. Rev. 136, B1187 (1964).

Measurement	Experiment	Accelerator	Weight/1000 (1 GeV/c ≤ p_{lab} <2 GeV/c)	Number of Momenta	Momentum Range (MeV/c)	Experimental Technique
π^+p DCS	Laasanen 73	ZGS	379	16	1207-2300	Wire chambers.
π^+p DCS	Hughes 72	Nimrod	302	18	800-1594	Acoustic chambers + single arm spectrometer.
π^+p DCS	Albrow 70	CERN PS	130	24	820-2740	Butanol target + counters.
π^+p DCS	Vavra 72	Bevatron	92	16	1250-2000	Double arm counter spectrometer, θ>125°.
π^+p DCS	Kalmus 71	Bevatron	66	8	1280-1840	72-inch and 25-inch HBC.
π^+p DCS	Rothschild 72	Bevatron	59	43	572-1628	Double arm counter spectrometer, θ=180°.
π^+p DCS	Duke 66	Nimrod	46	12	875-1579	Counters.
π^-p DCS	Crabb 71	Bevatron	137	33	600-1280	Double arm counter spectrometer, θ>155°.
π^-p DCS	Ott 72	Bevatron	99	31	1280-3000	Double arm counter spectrometer, θ>125°.
π^-p DCS	Aplin 71	Nimrod	86	31	1210-2940	Counters.
π^-p DCS	Broome 73	Nimrod	79	16	996-1342	Counters.
π^-p DCS	Albrow 72	CERN PS	63	16	865-2632	LMN and butanol targets + counters.
π^-p DCS	Duke 66	Nimrod	61	13	875-1579	Counters.
π^-p DCS	Abillon 70	Saturne	30	15	875-1580	Double arm chamber spectrometer, θ near 180°.
π^-p DCS	Brody 71	ZGS/Bevatron	26	35	557-1604	30-inch/72-inch HBC's.
π^-p DCS	Fellinger 70	ZGS	23	18	1710-5530	Double arm counter spectrometer, $\|t\|$<.8 $(GeV/c)^2$.
CEX DCS	Nelson 73	Bevatron	20	6	1030-2390	Optical chambers.
CEX DCS	Chiu 67	Bevatron	7	9	624-1433	Optical chambers.
CEX DCS	Bulos 69	Cosmotron	5	11	654-1247	Optical chambers.
CEX DCS	Risk 68	PPA	1.3	15	561-2106	Optical chambers, θ=0°.
CEX DCS	Kistiakowsky 72	ZGS	1.0	52	1800-6000	Shower counter + neutron counter, θ=180°.
CEX DCS	Carroll 69	Nimrod	0.6	5	1715-2460	Optical chambers.
CEX DCS	Borgeaud 64	Saturne	0.5	15	894-1995	Optical chambers, θ=0°.
π^+p POL	Martin 74	Nimrod	1751	68	603-2651	LMN target + counters.
π^+p POL	Albrow 70	CERN PS	286	24	820-2740	Butanol target + counters.
π^+p POL	Burleson 71	ZGS	62	4	1600-2310	Ethelyne glycol target + counters.
π^+p POL	Chamberlain 66	Bevatron	22	15	745-3747	LMN target + counters.
π^-p POL	Hill 71	ZGS	301	5	1600-2280	Ethelyne glycol target + counters.
π^-p POL	Albrow 72	CERN PS	112	16	865-2632	LMN and butanol targets + counters.
π^-p POL	Cox 69	Nimrod	53	50	643-2140	LMN target + counters.
π^-p POL	Duke 68	Nimrod	10	8	875-1579	LMN target + counters.
π^-p POL	Hill 70	ZGS	6	5	1700-2500	LMN target + counters.
π^-p POL	Chamberlain 66	Bevatron	6	11	596-3260	LMN target + counters.
CEX POL	Shannon 74	Bevatron	6	5	1030-1790	Propylene glycol target + optical chambers.

Table I. A survey of the main elastic and CEX scattering experiments in the 1-2 GeV/c momentum range.[4]

DATA POINT CONFIDENCE LEVEL DISTRIBUTION

1.00 - .95	XXXXX	22
.95 - .90	XXXXX	24
.90 - .85	XXXXX	25
.85 - .80	XXX	14
.80 - .75	XXXXXX	26
.75 - .70	XXXX	20
.70 - .65	XXXXXX	30
.65 - .60	XXXXX	24
.60 - .55	XXXX	16
.55 - .50	XXXXX	22
.50 - .45	XXXXX	25
.45 - .40	XXXX	18
.40 - .35	XXXXX	24
.35 - .30	XXXXXX	30
.30 - .25	XXXX	20
.25 - .20	XXXX	16
.20 - .15	XXXXXX	26
.15 - .10	XXXXXXX	32
.10 - .05	XXXXXXXXX	42
.05 -0.00	XXXXXXXXXXXXXXX	72

.050 - .045	XX	2
.045 - .040	XXXXXXX	7
.040 - .035	XX	2
.035 - .030	XXXXXXX	7
.030 - .025		0
.025 - .020	XXXXXXXX	8
.020 - .015	XXXXXX	6
.015 - .010	XXXXXXXX	8
.010 - .005	XXXXXXXX	8
.005 -0.000	XXXXXXXXXXXXXXXXXXXXXXXX	24

DATA BLOCK CONFIDENCE LEVEL DISTRIBUTION

1.0 - .9		0
.9 - .8		0
.8 - .7		0
.7 - .6		0
.6 - .5		0
.5 - .4		0.
.4 - .3	X	1
.3 - .2		0
.2 - .1	X	1
.1 -0.0	XXXXXXXXXX	10

.10 - .09		0
.09 - .08		0
.08 - .07		0
.07 - .06		0
.06 - .05		0
.05 - .04		0
.04 - .03		0
.03 - .02		0
.02 - .01	X	1
.01 -0.00	XXXXXXXXX	9

DATA POINT CONFIDENCE LEVEL DISTRIBUTION

1.00 - .95	XXXX	19
.95 - .90	XXXXX	24
.90 - .85	XXXXX	22
.85 - .80	XXXXXX	28
.80 - .75	XXXXX	23
.75 - .70	XXXX	17
.70 - .65	XXXXXX	28
.65 - .60	XXXXXX	27
.60 - .55	XXXX	18
.55 - .50	XXXXX	25
.50 - .45	XXXXX	25
.45 - .40	XXXXXX	29
.40 - .35	XXXXX	24
.35 - .30	XXXXX	22
.30 - .25	XXXXX	25
.25 - .20	XXXXXXX	35
.20 - .15	XXXXXXX	34
.15 - .10	XXXXXXX	32
.10 - .05	XXXXXXXXXXX	51
.05 -0.00	XXXX	20

.050 - .045	XXXX	4
.045 - .040	XXXXXX	6
.040 - .035	XXXXX	5
.035 - .030	X	1
.030 - .025	X	1
.025 - .020	XX	2
.020 - .015		0
.015 - .010		0
.010 - .005	X	1
.005 -0.000		0

DATA BLOCK CONFIDENCE LEVEL DISTRIBUTION

1.0 - .9		0
.9 - .8		0
.8 - .7	XXX	3
.7 - .6		0
.6 - .5	X	1
.5 - .4	X	1
.4 - .3	XX	2
.3 - .2		0
.2 - .1	XXXXX	5
.1 -0.0		0

.10 - .09	0
.09 - .08	0
.08 - .07	0
.07 - .06	0
.06 - .05	0
.05 - .04	0
.04 - .03	0
.03 - .02	0
.02 - .01	0
.01 -0.00	0

XBL 747-1151

Fig. 1. Chi-squared confidence level distributions from an amalgamation of π^+p DCS data at 1590 MeV/c. The distributions after the first (second) pass fit are shown on the left (right). The numbers of data points or blocks in each confidence interval is given to the right of the histograms; there is a total of 528 data points and 12 data blocks. In each case the lowest confidence interval bin is also shown on an expanded scale. After the first pass 76 errors (including 3 normalization and 2 momentum errors) were enlarged, 43 of these by less than a factor of 1.5. An additional 16 errors were enlarged after the second pass, all but one by less than a factor of 1.5. The overall χ^2 per degree of freedom was 1.82 after the first pass and 1.07 after the second pass.

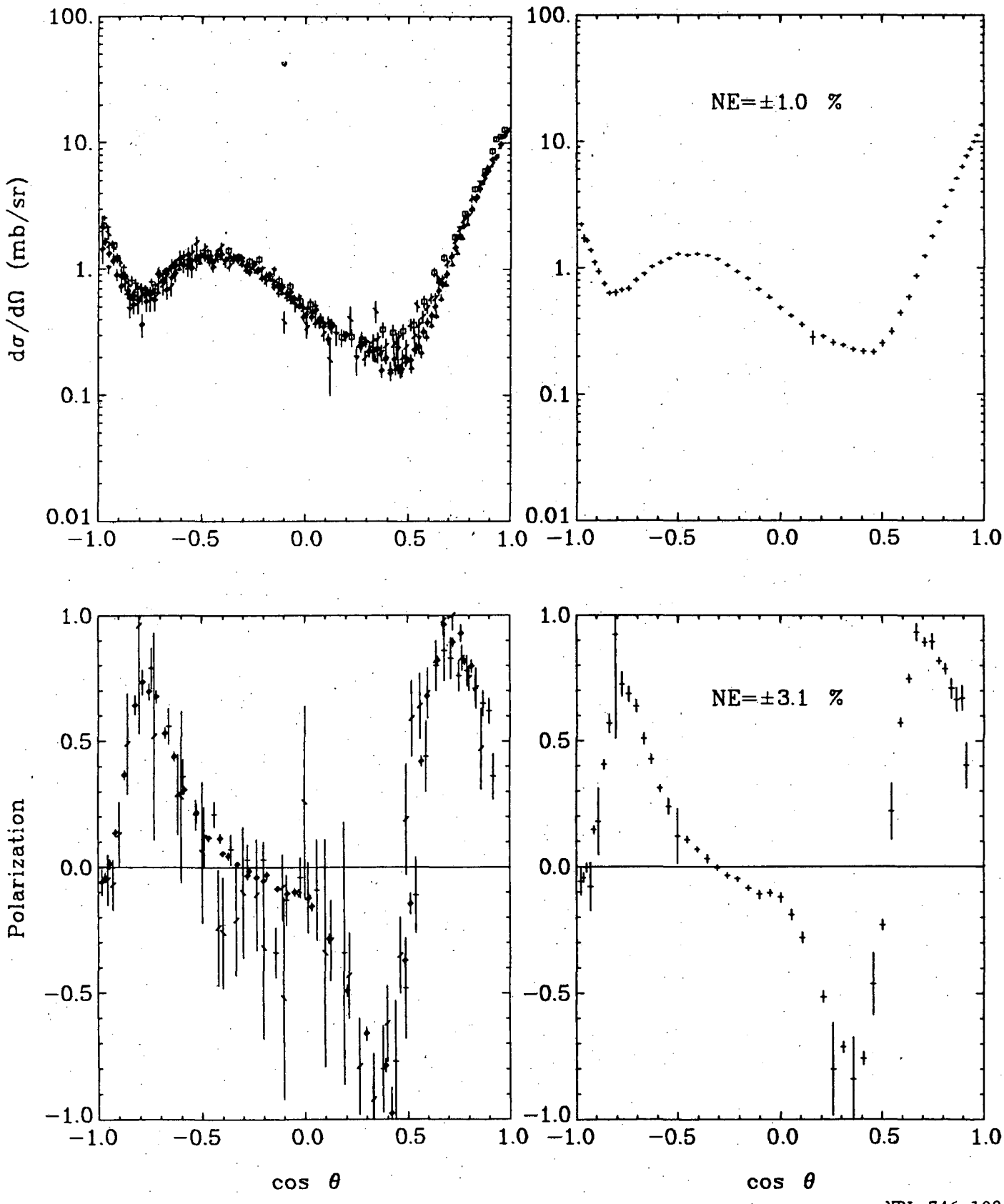

XBL 746-1080

Fig. 2. Amalgamation of π^+p elastic scattering data at 1437 MeV/c. The input data in the central momentum bin (1420-1465 MeV/c) is shown on the left; amalgamated data at 1437 MeV/c is shown on the right.

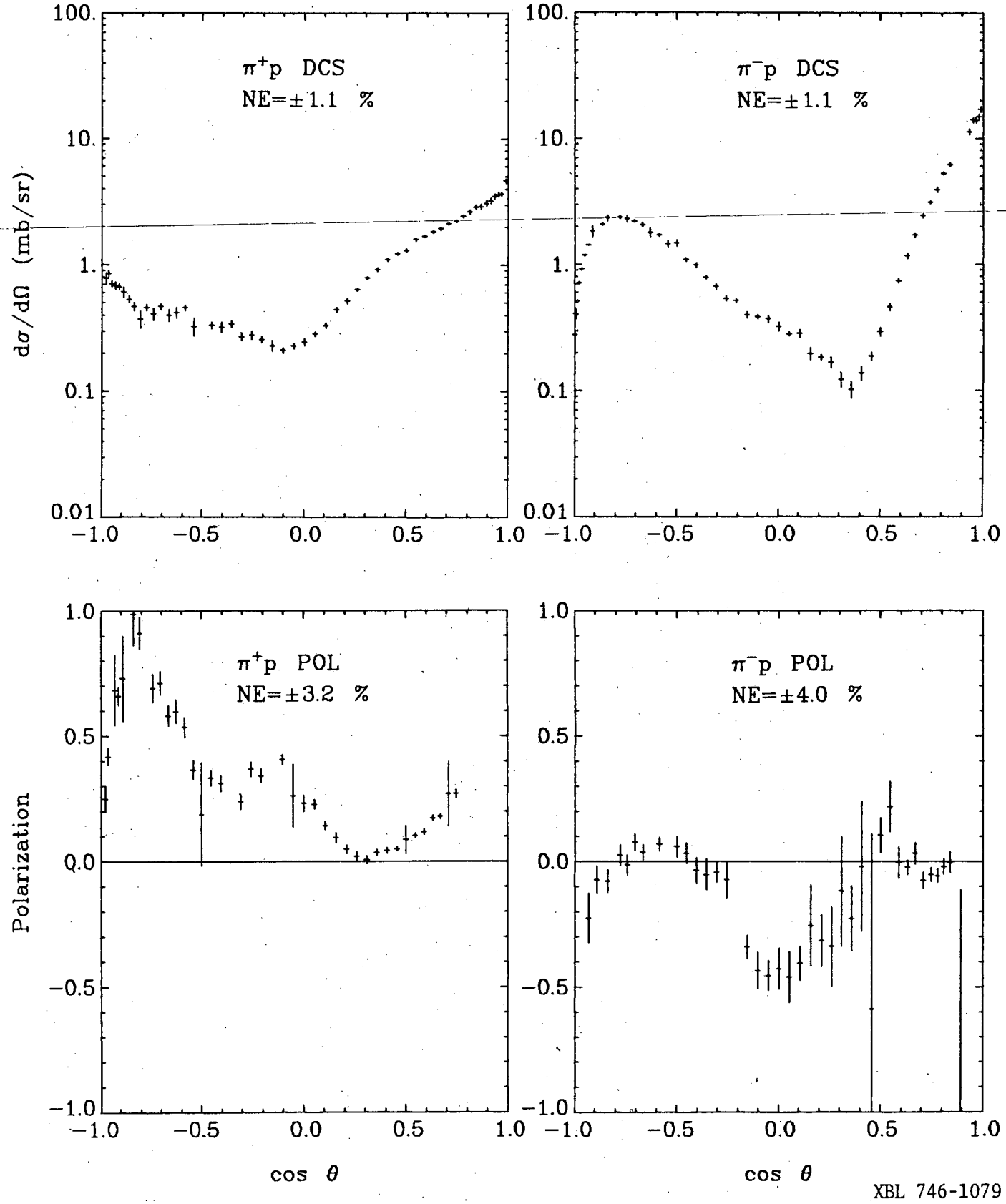

XBL 746-1079

Fig. 3. Amalgamated elastic scattering data at 1030 MeV/c. The data types and normalization errors are indicated on the graphs.

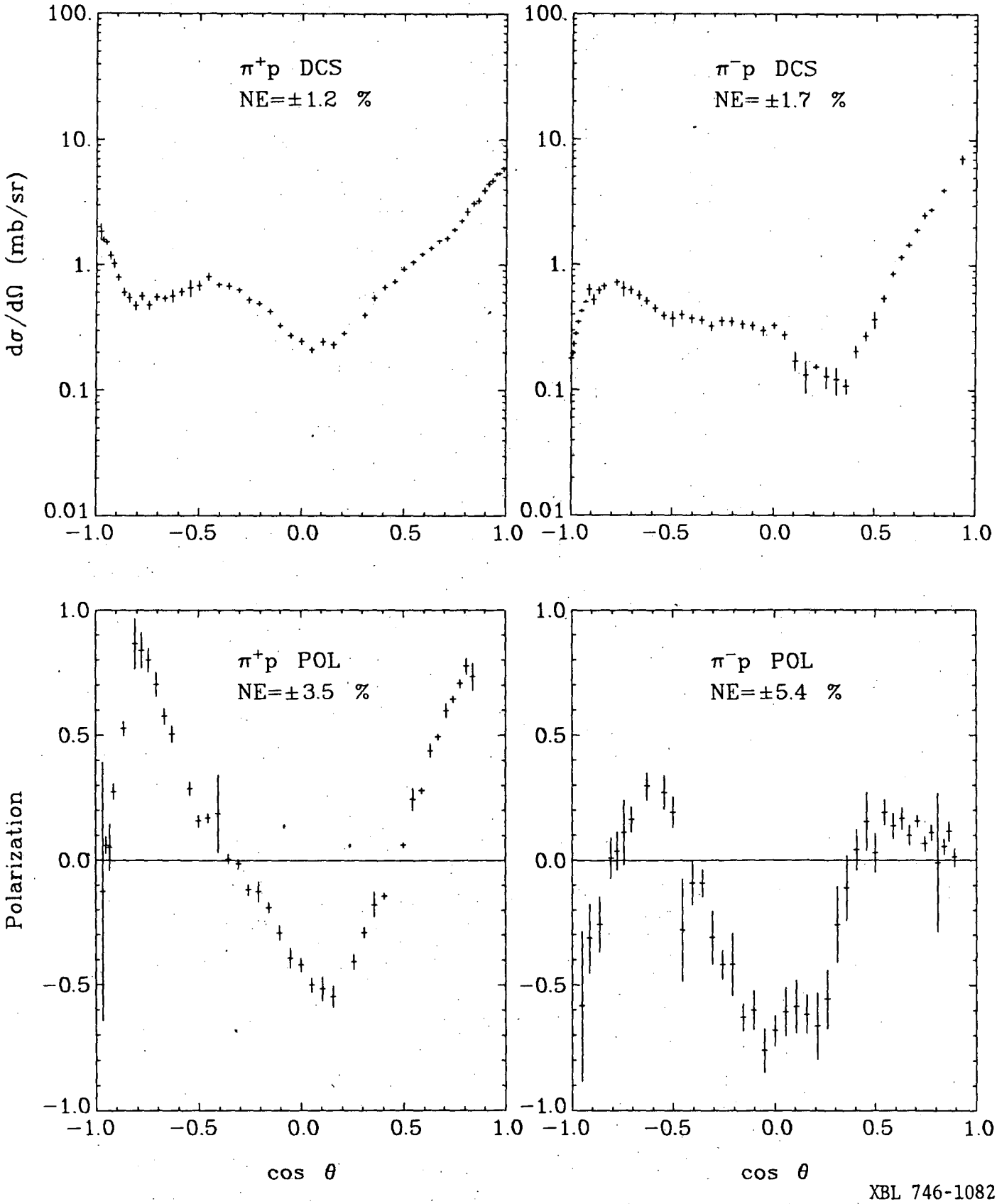

XBL 746-1082

Fig. 4. Amalgamated elastic scattering data at 1247 MeV/c. The data types and normalization errors are indicated on the graphs.

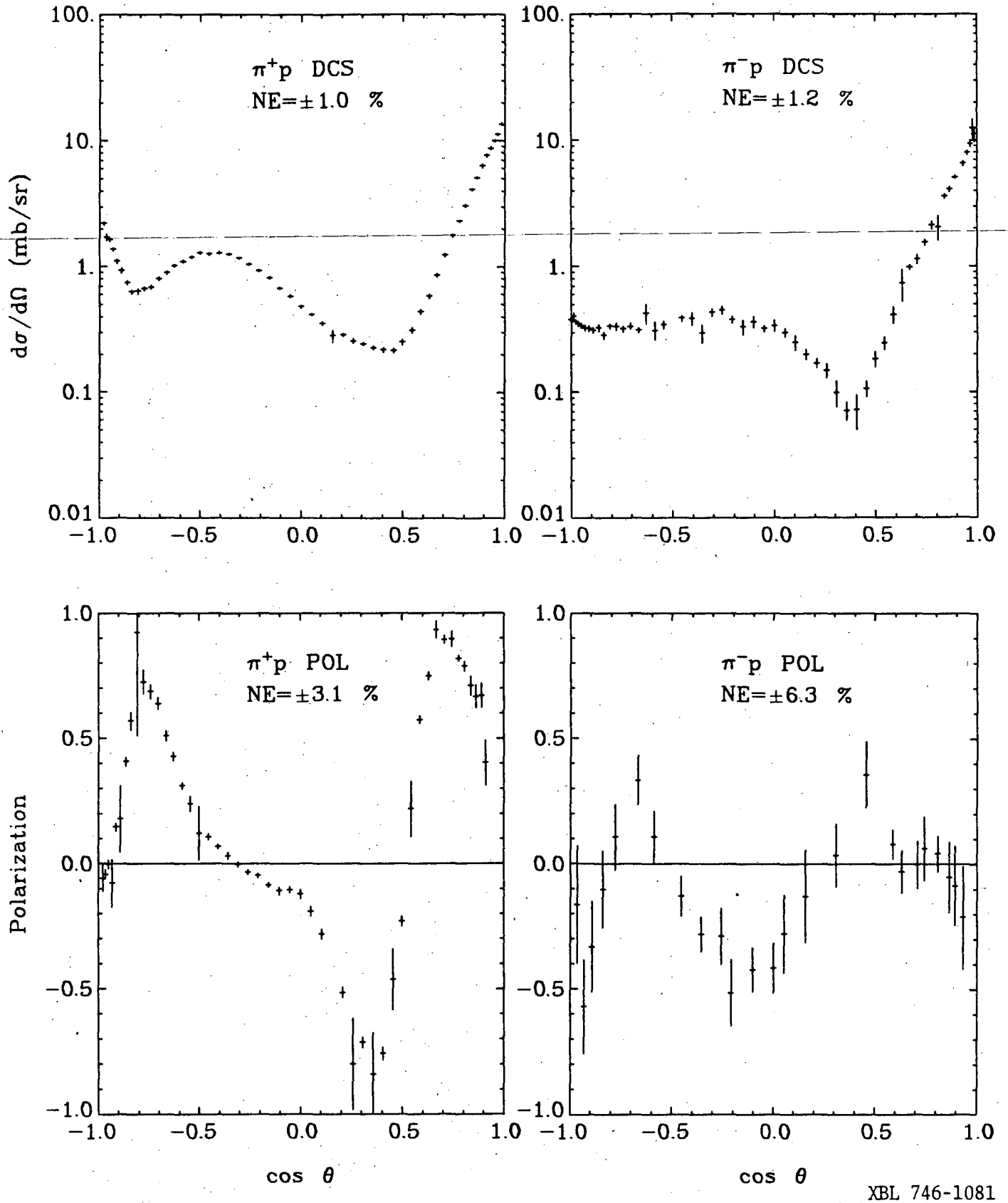

XBL 746-1081

Fig. 5. Amalgamated elastic scattering data at 1437 MeV/c. The data types and normalization errors are indicated on the graphs.

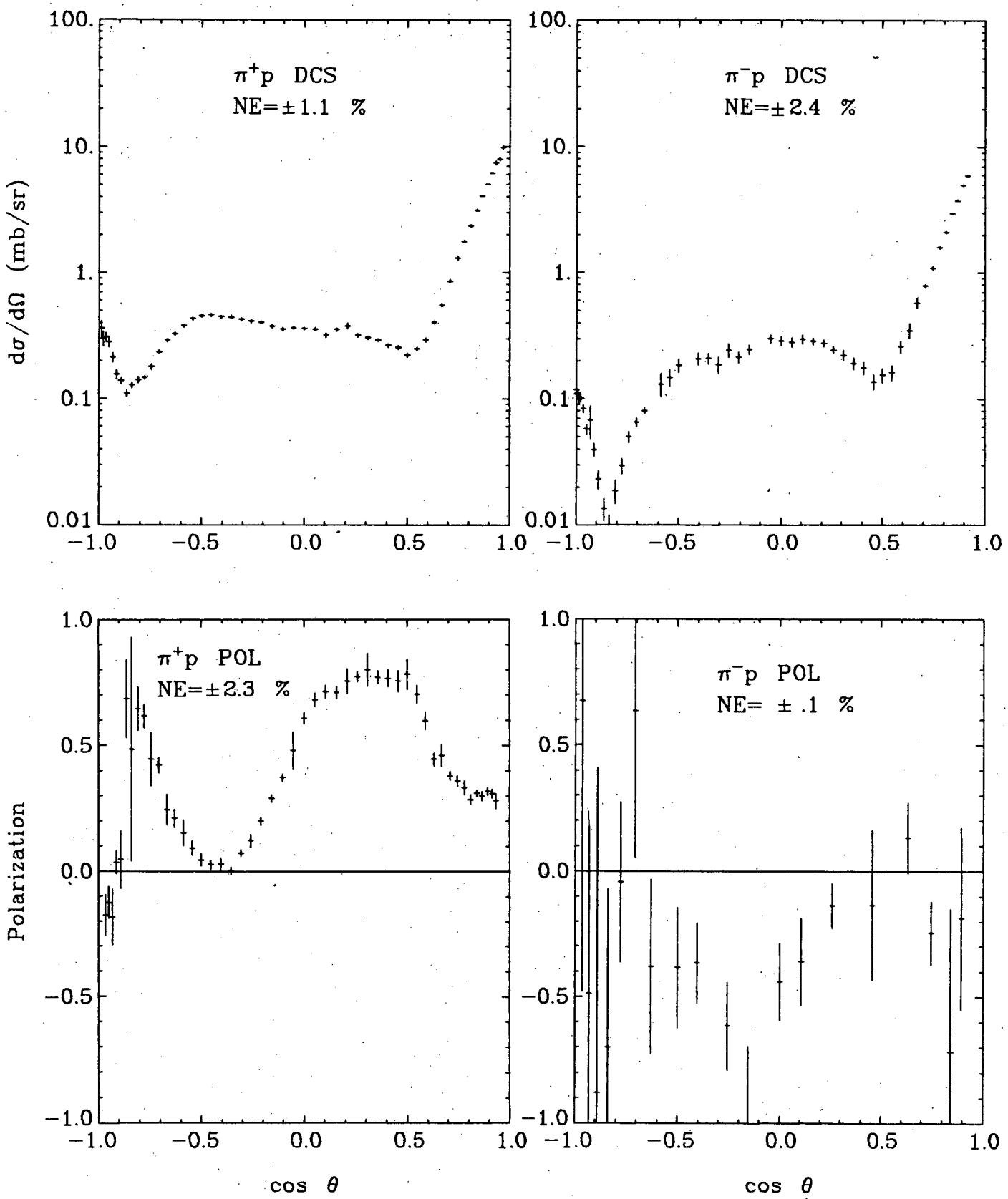

XBL 746-1084

Fig. 6. Amalgamated elastic scattering data at 1790 MeV/c. The data types and normalization errors are indicated on the graphs.

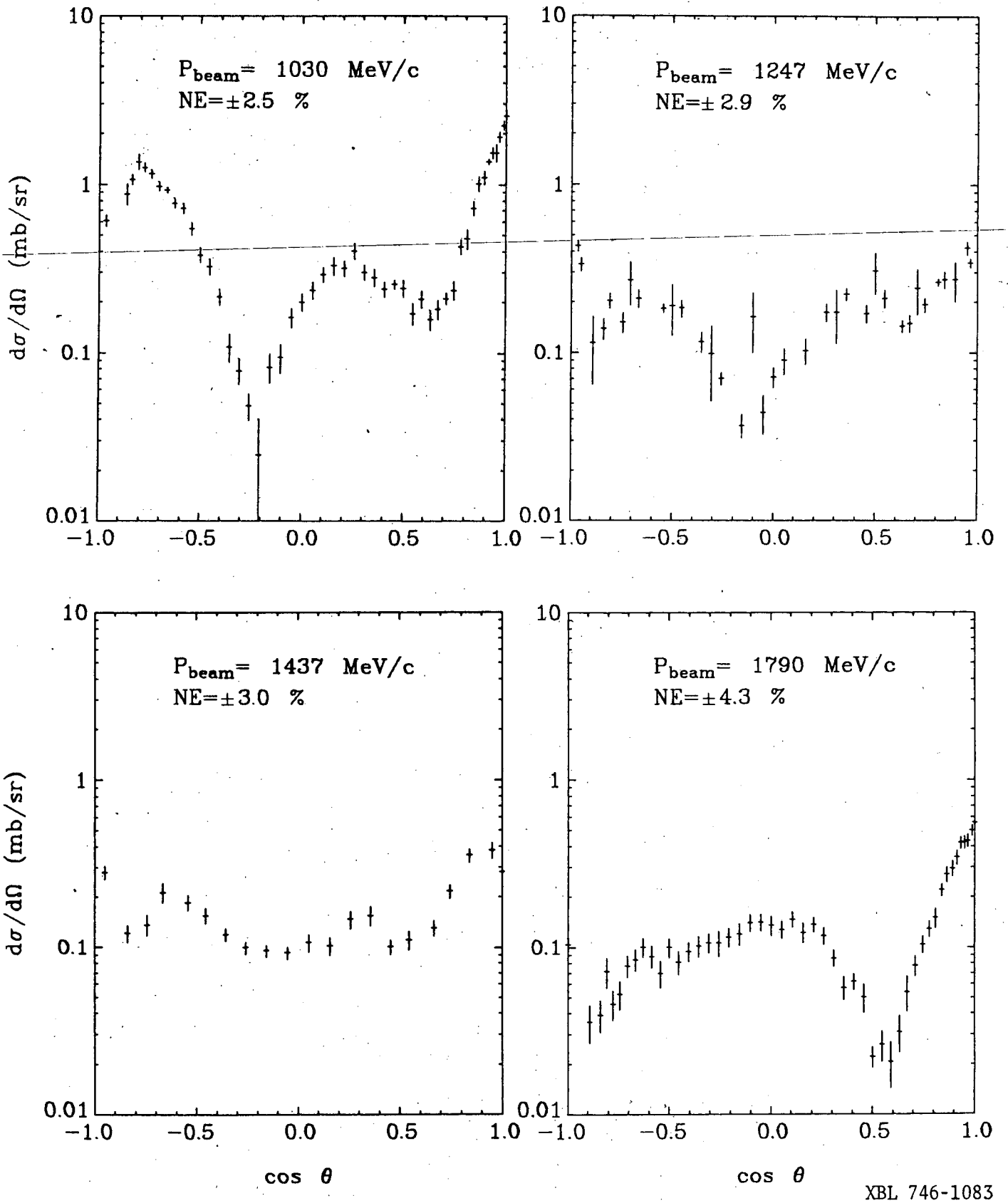

XBL 746-1083

Fig. 7. Amalgamated CEX cross-section data. The beam momenta and normalization errors are indicated on the graphs.

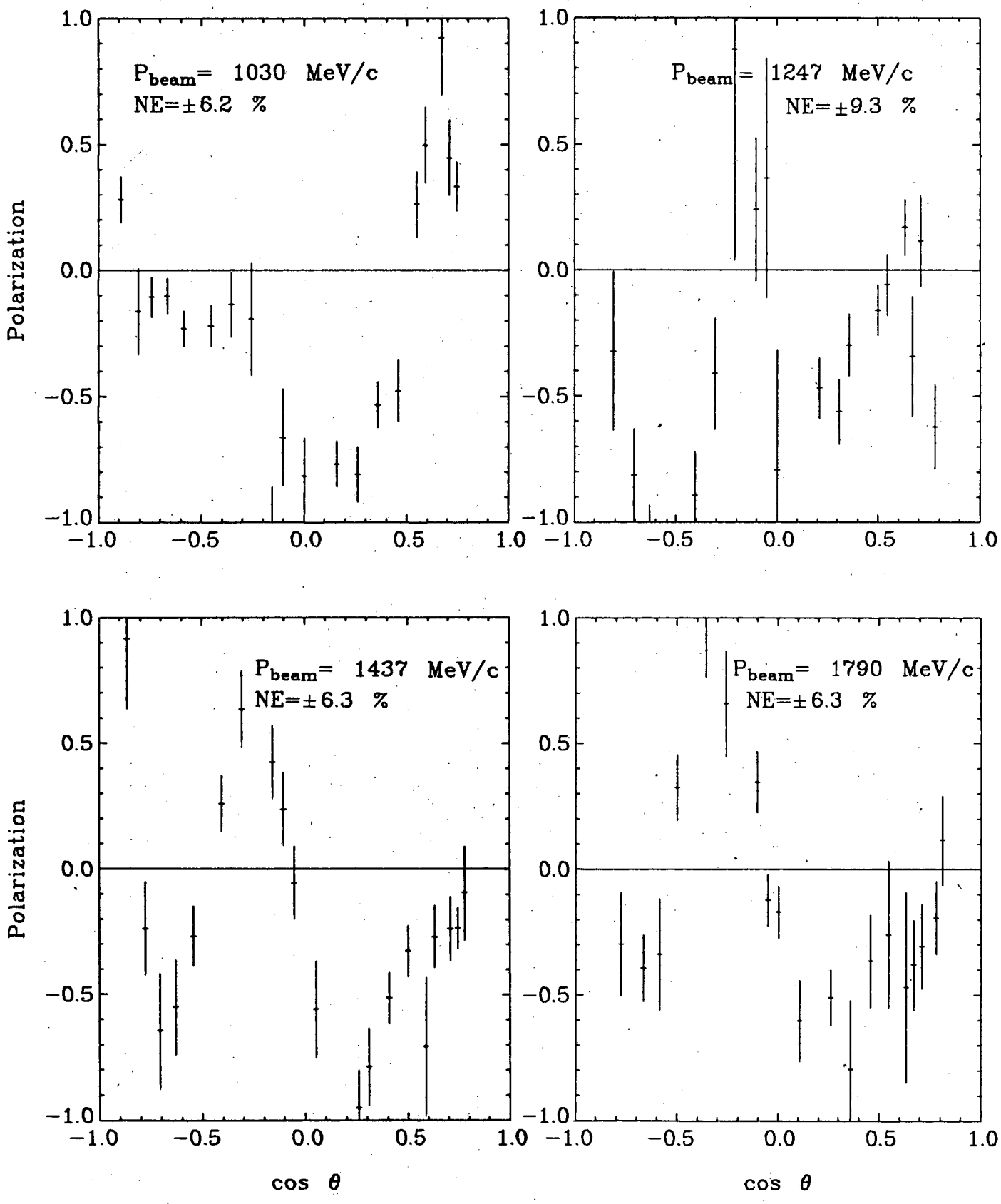

XBL 746-1085

Fig. 8. Amalgamated CEX polarization data. The beam momenta and normalization errors are indicated on the graphs.

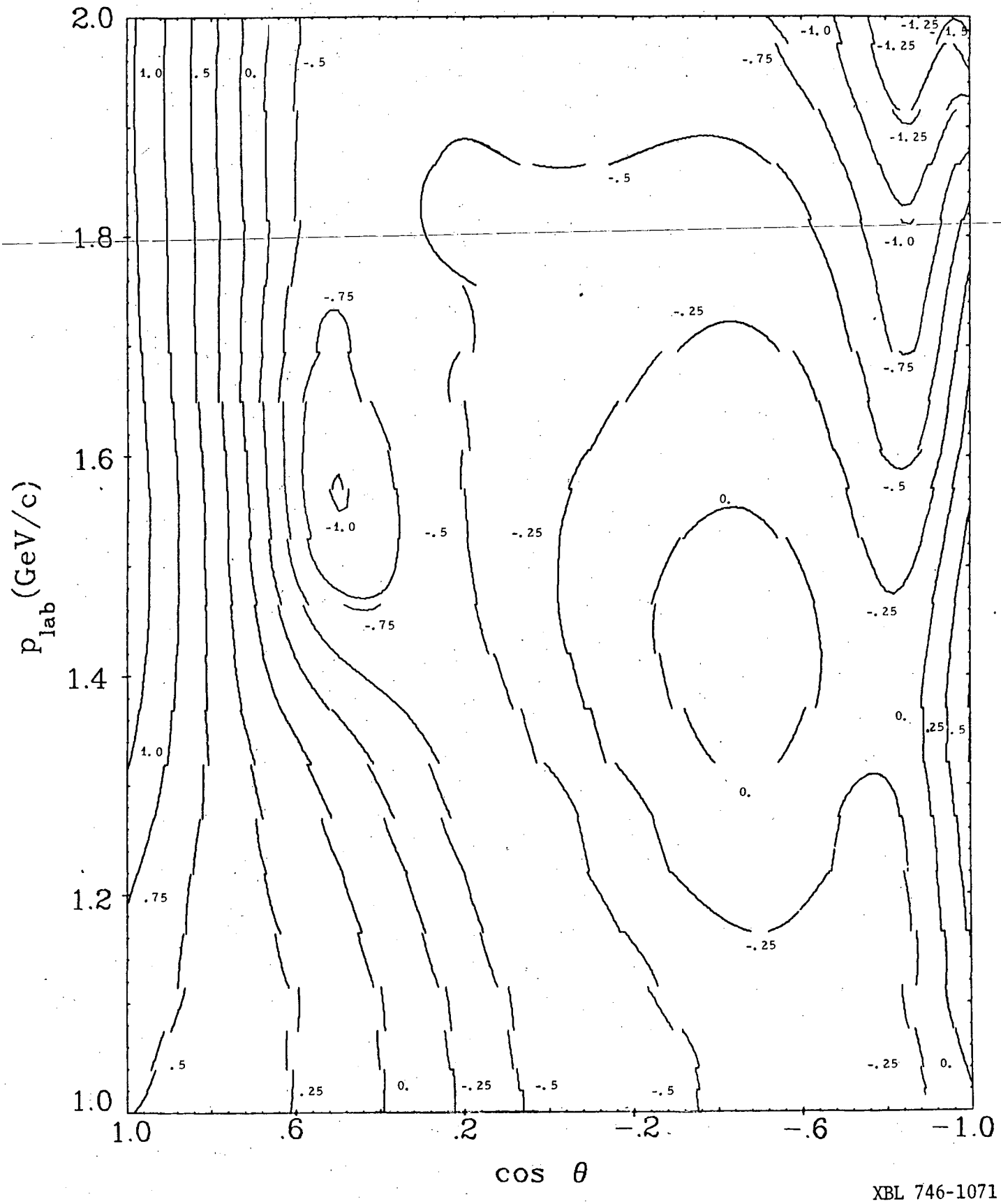

Fig. 9. Contour map of log dσ/dΩ (mb/ster) for π^+p elastic scattering. The contour line spacing is one quarter of a decade.

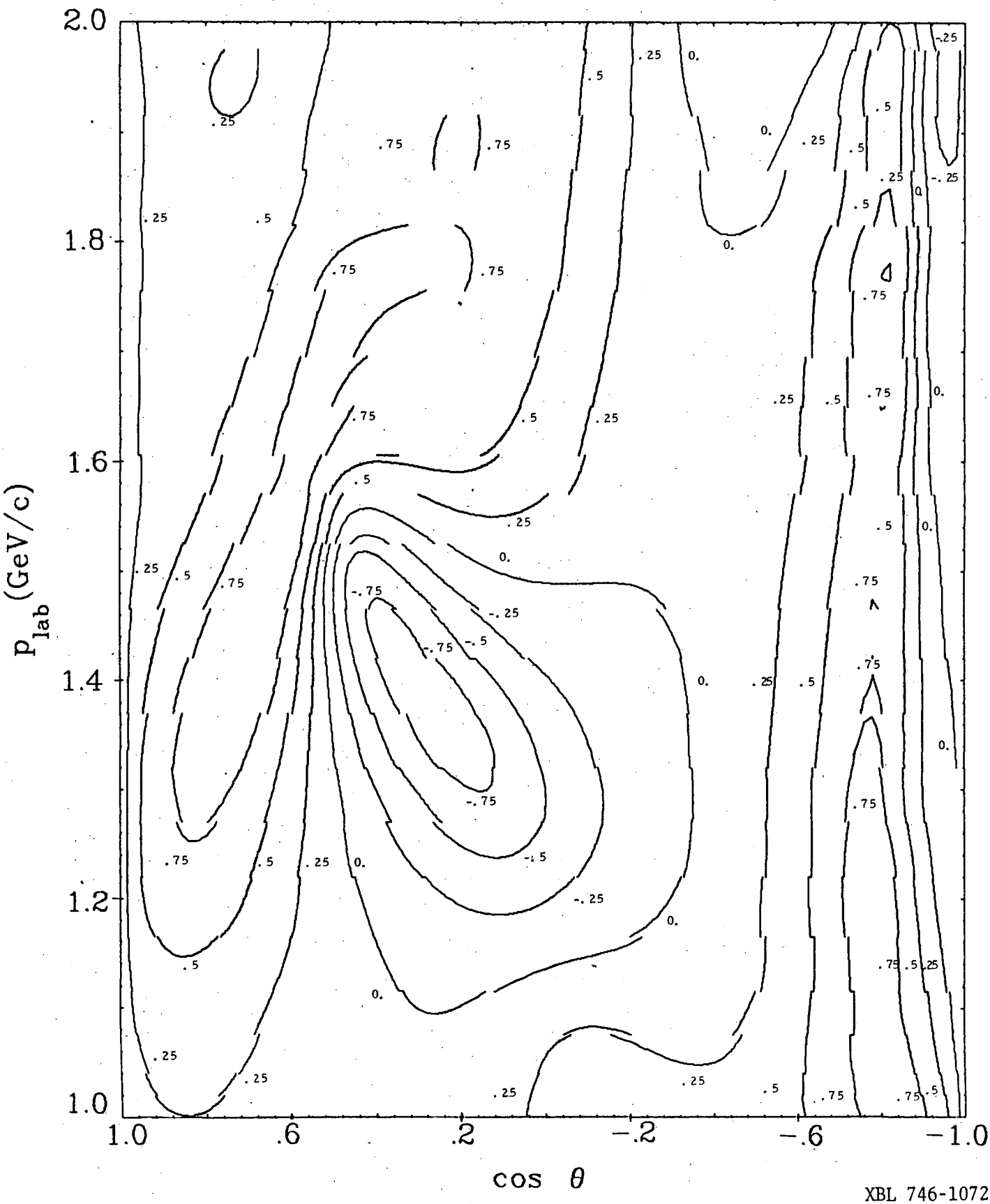

Fig. 10. Contour map of the $\pi^+ p$ elastic polarization. The contour line spacing is 0.25.

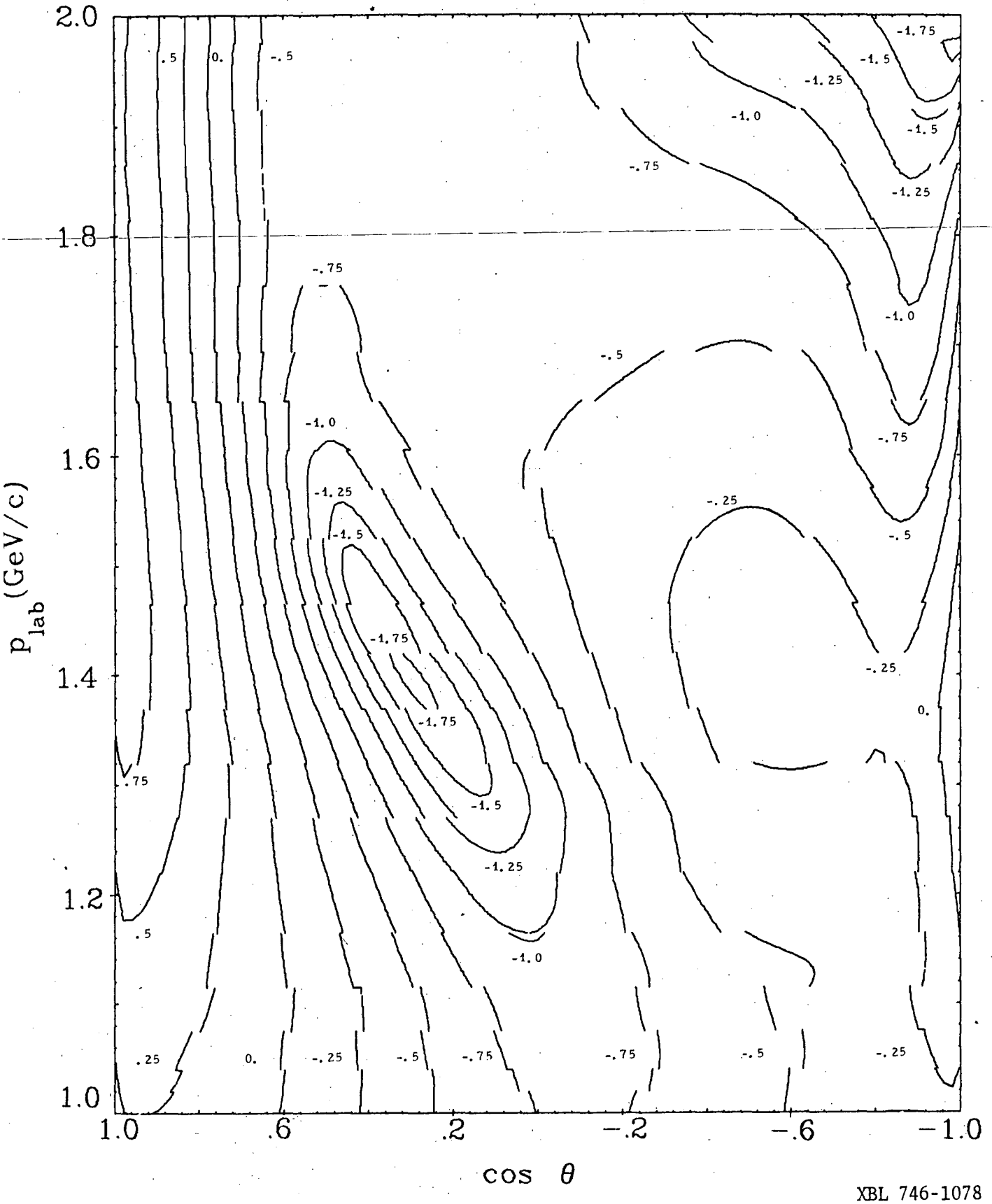

XBL 746-1078

Fig. 11. Contour map of log I_+ (mb/ster) for $\pi^+ p$ elastic scattering. The contour line spacing is one quarter of a decade.

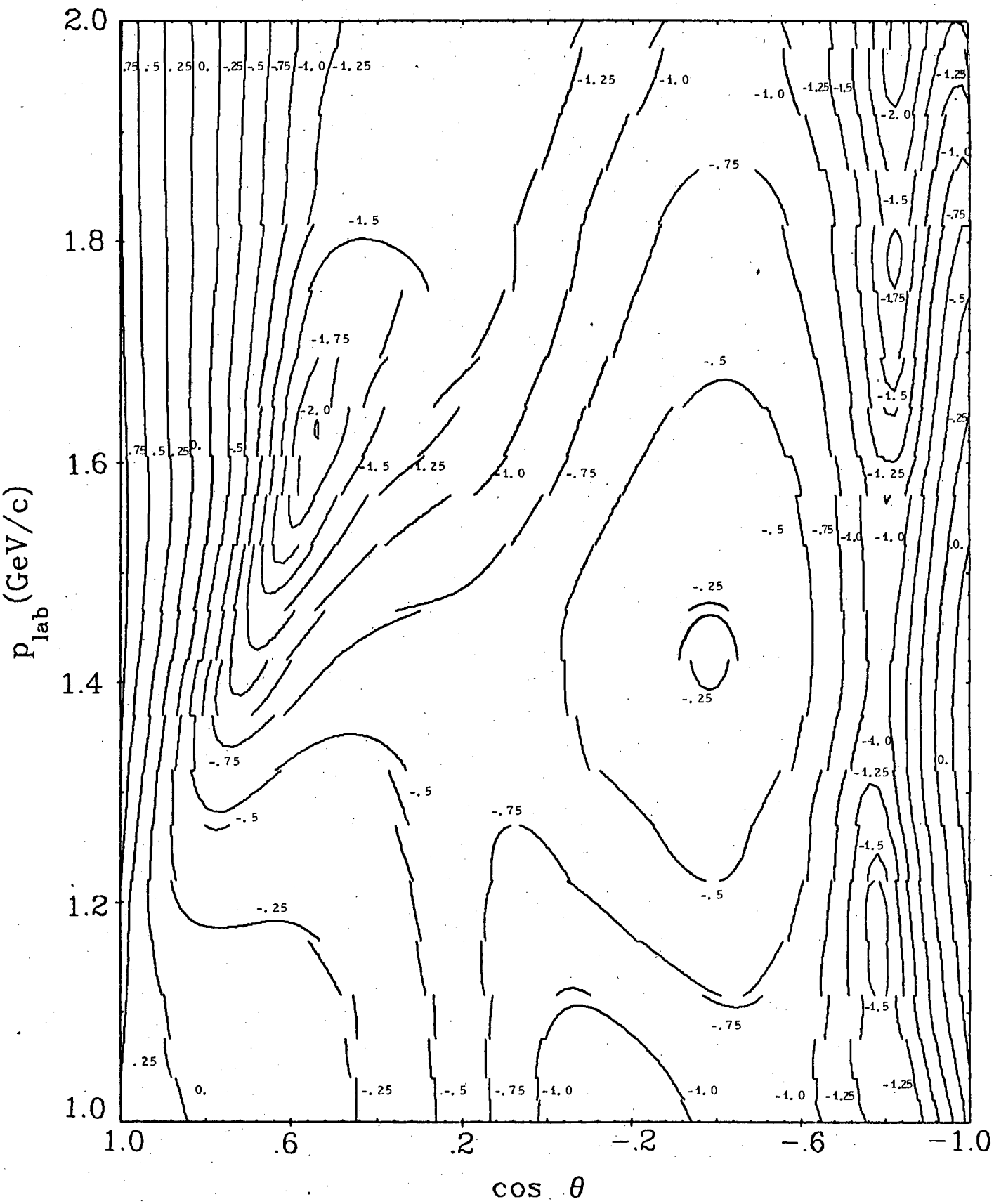

XBL 746-1077

Fig. 12. Contour map of log I_- (mb/ster) for $\pi^+ p$ elastic scattering. The contour line spacing is one quarter of a decade.

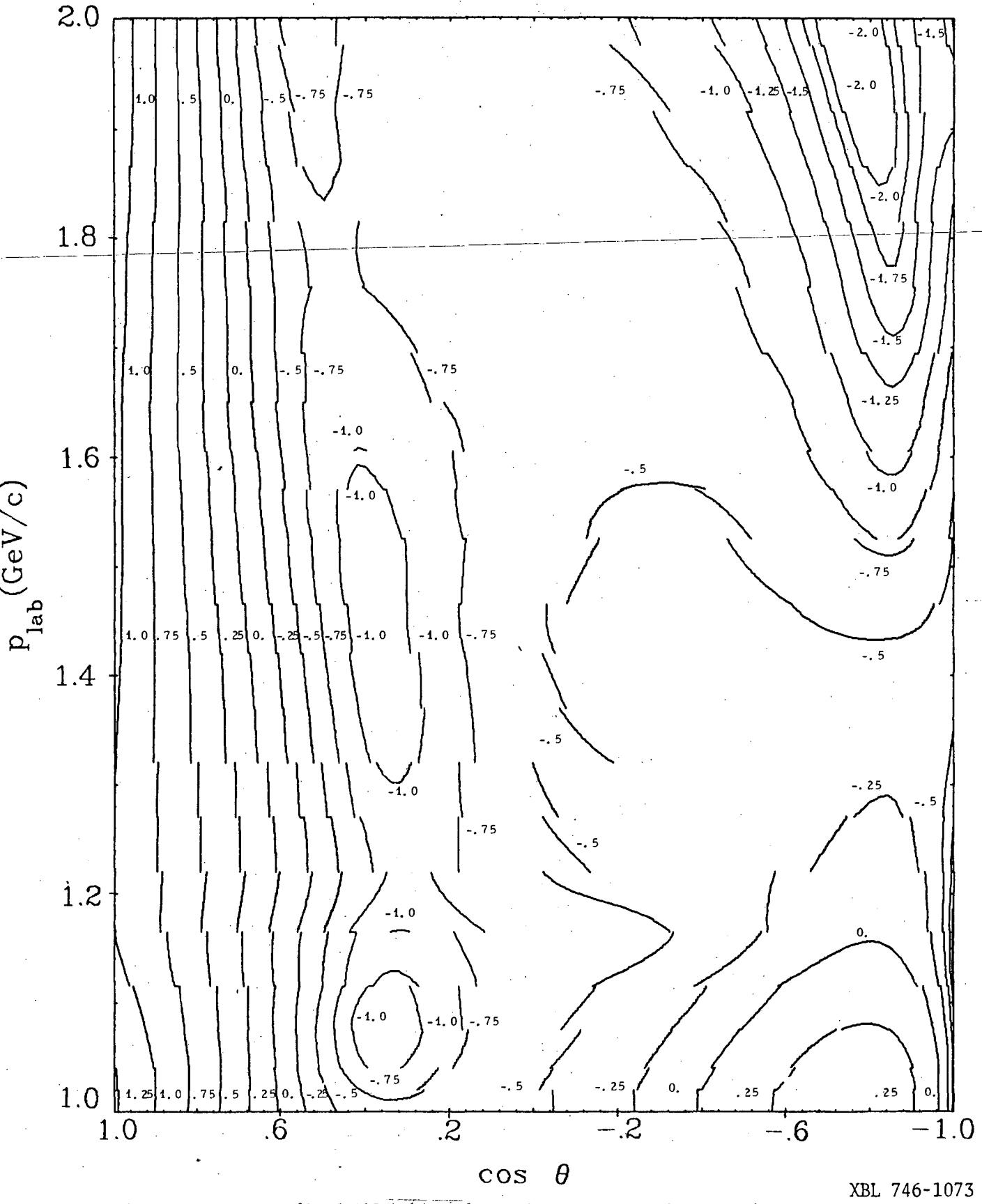

XBL 746-1073

Fig. 13. Contour map of log dσ/dΩ (mb/ster) for π^-p elastic scattering. The contour line spacing is one quarter of a decade.

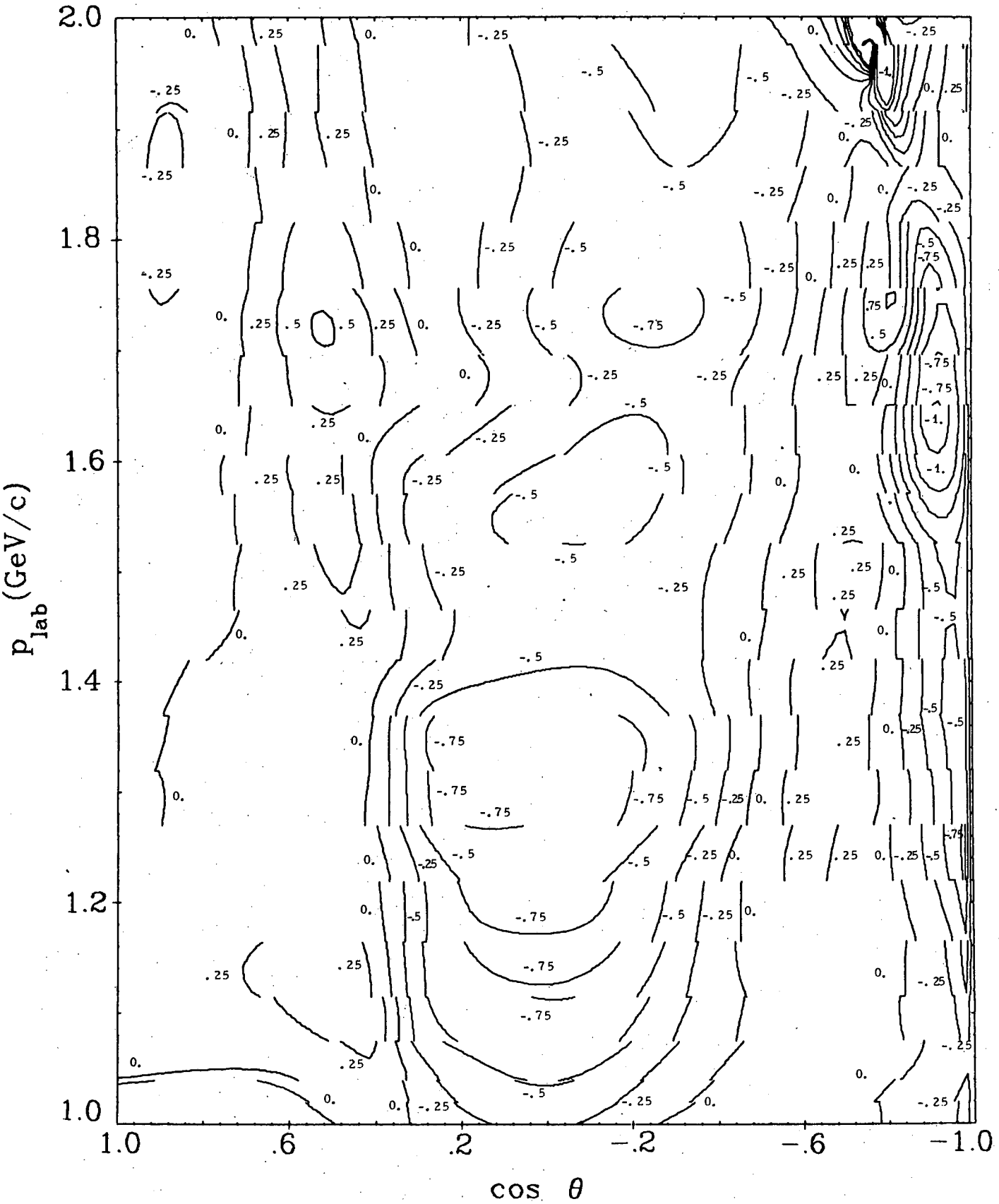

XBL 746-1076

Fig. 14. Contour map of the $\pi^- p$ elastic polarization. The contour line spacing is 0.25.

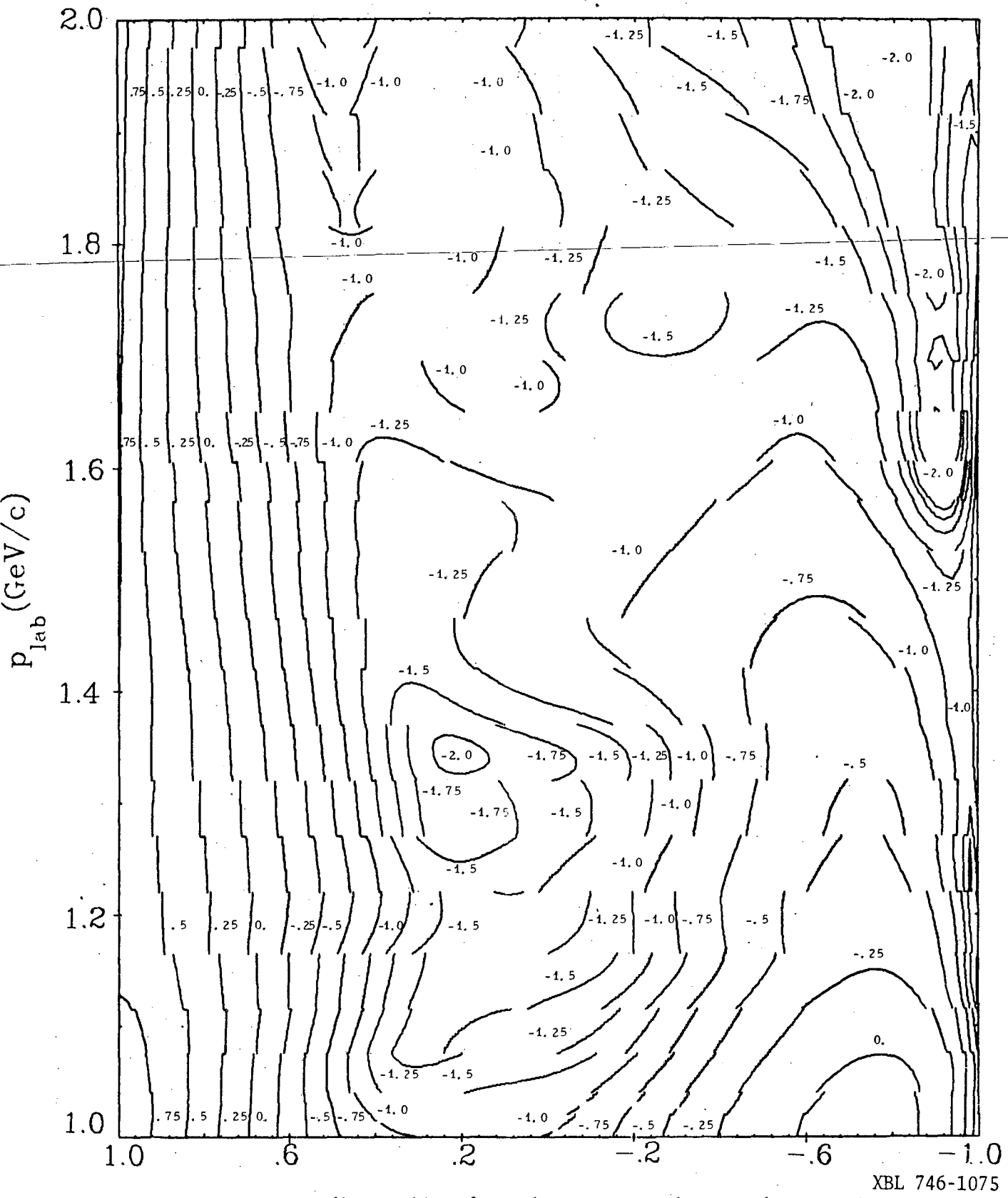

Fig. 15. Contour map of log I_+ (mb/ster) for $\pi^+ p$ elastic scattering. The contour line spacing is one quarter of a decade.

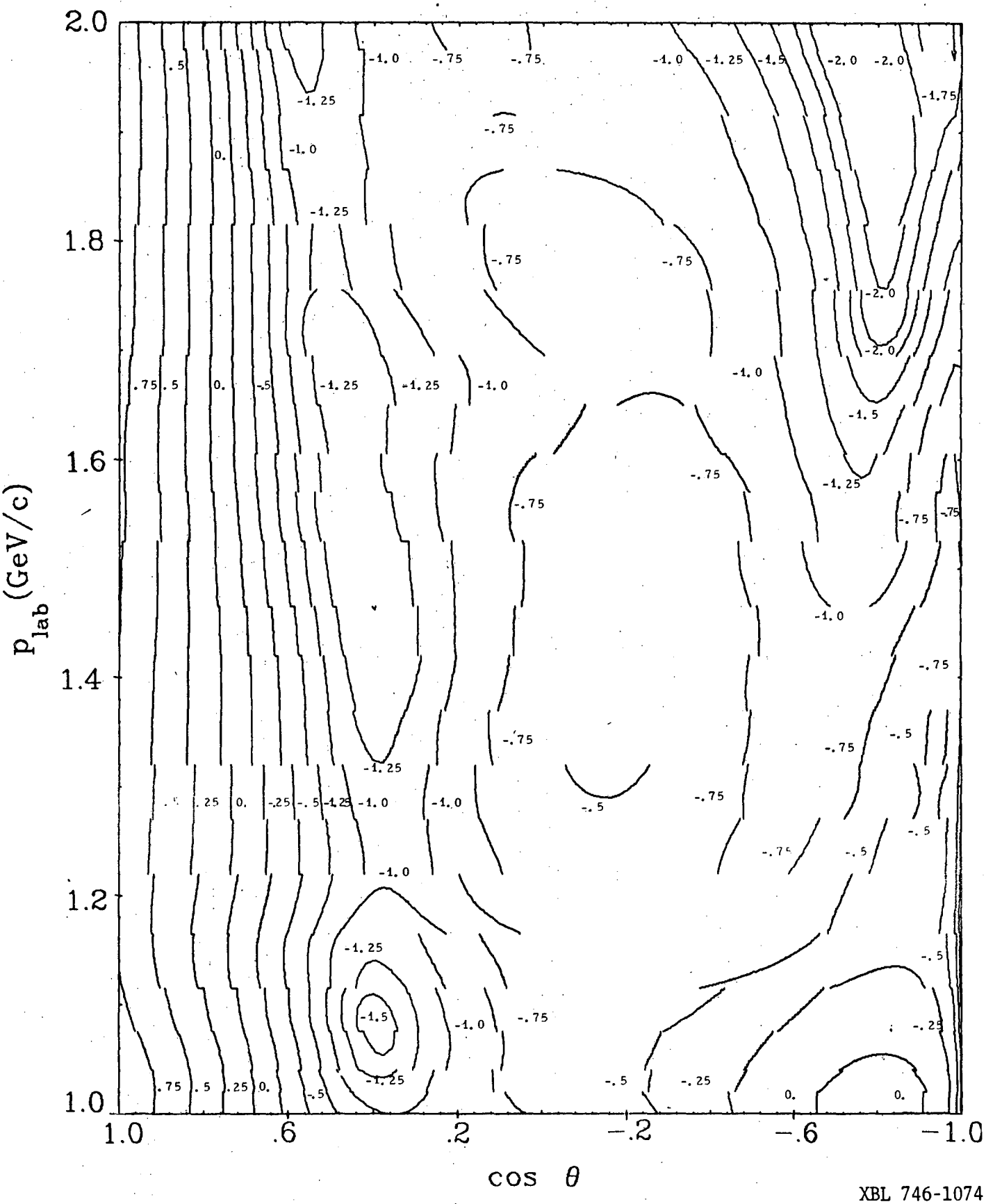

XBL 746-1074

Fig. 16. Contour map of log I_- (mb/ster) for π^-p elastic scattering. The contour line spacing is one quarter of a decade.

TECHNICAL INFORMATION DIVISION
LAWRENCE BERKELEY LABORATORY
UNIVERSITY OF CALIFORNIA
BERKELEY, CALIFORNIA 94720